# Powder Bed Layer Characteristics – The Overseen First Order Process Input

H.-W. Mindt
ESI Software Germany

M. Megahed
**Corresponding author**
**ESI Software Group**
**Email: mme@esi-group.com**

N.P. Lavery
Swansea University, United Kingdom

M.A. Holmes,
Swansea University, United Kingdom

S.G.R. Brown
Swansea University, United Kingdom

## Keywords
Additive Manufacturing, Powder Bed Modelling, Powder Coating, Powder Bed Packing Density

## Abstract
Powder Bed Additive Manufacturing offers unique advantages in terms of manufacturing cost, lot size and product complexity compared to traditional processes such as casting, where a minimum lot size is mandatory to achieve economic competitiveness. Many studies – both experimental and numerical - are dedicated to the analysis of how process parameters such as heat source power, scan speed and scan strategy affect the final material properties. Apart from the general urge to increase the build rate using thicker powder layers, the coating process and how the powder is distributed on the processing table has receive27d very little attention to date. This paper focuses on the first step of every powder bed build process: Coating the process table. A numerical study is performed to investigate how powder is transferred from the source to the processing table. A solid coating blade is modelled to spread commercial Ti-6Al-4V powder. The resulting powder layer is analyzed statistically to determine the packing density and its variation across the processing table. The results are compared with literature reports using so called “rain” models. A parameter study is performed to identify the influence of process table displacement and wiper velocity on the powder distribution. The achieved packing density and how that affects subsequent heat source interaction with the powder bed is also investigated numerically.

## Introduction

Powder Bed Additive Manufacturing is a form of Additive Manufacturing (AM) that deposits very thin layers of metal powder (microns). A heat source (laser or electron beam) melts the metallic powder in certain areas of the powder bed. These areas then solidify to become a section of the final build. An additional powder layer is added, and the process is repeated. At the end of the build process unprocessed powder is removed to reveal the final product.

There are a large number of control parameters that interact in a complex manner affecting the final product quality [1. A large amount of research has been reported investigating the energy absorption of the powder bed [2,3], melt pool characteristics [4,5,6,7,8] thermal evolution of the build, residual stresses and final work piece distortion [6, 9,10,11,12,13,14,15,16,17]. In spite of the general acceptance that the powder quality is a key factor in the overall process and the final product quality [18,19], very little attention had been paid to the powder coating process and the characteristics of the powder bed.

When referencing powder layer thickness, we distinguish three different values:

1. Processing table displacement is the vertical motion of the processing table prior to the application of a new powder layer. It is chosen / set by the machine operator at the beginning of the build processes. The processing table displacement is often wrongly used to quantify the powder layer thickness, as will be discussed below.
2. Powder layer thickness is the thickness of the newly coating powder layer. It corresponds to the minimum depth the heat source must penetrate to achieve bonding of the new layer with the based material.
3. Consolidated layer thickness is the height of the processed powder material (deposited material).

We relate the different layer thicknesses to one another via the powder bed packing density. When a newly coated layer is processed the thickness will decrease proportionally to the packing density as the material melts and solidifies again:

$$\delta_c = \delta_p \rho_p \qquad (1)$$

where $\delta_c$ is the consolidated powder layer thickness after laser processing, $\delta_p$ is the fresh powder layer thickness and $\rho_p$ is the packing density of the fresh powder layer. The volume remaining after material consolidation and prior to displacing the processing table again leads to a larger powder layer thickness. The table downward displacement $\delta_t$ is added to the free height above the processed material to obtain the new powder layer thickness:

$$\delta_{p|_{n+1}} = \delta_{t|_{n+1}} + \delta_{p|_n}\left(1 - \rho_{p|_n}\right) \qquad (2)$$

where *n* and *n+1* denote the previous and new layer respectively.

Assuming a uniform powder packing density of 50% and that the final build porosity is negligible; Figure 1 shows how the powder layer thickness evolves from one layer to the other. It can be seen that within 7 table displacements, the powder layer thickness reaches a steady value that is twice the table displacement.

Figure 2 shows how the packing density affects the powder layer thickness assuming a constant processing table displacement. The final powder layer thickness is inversely proportional to the packing density. It is also interesting to note that a lower packing density retards the achievement of a steady powder layer thickness. Mindt et al. showed how the powder layer thickness interacts with laser scan speed and hatch spacing in a complex manner influencing the final build porosity and quality [7,8]. Together with the large differences in powder layer thickness shown in Figure 2 it is apparent that better estimates of powder bed packing density are needed in order for powder bed models to be able to predict the final build porosity.

We developed a numerical tool to analyze particle motion during the coating process. The powder particles are assumed to be spheres. Each particle is assigned a certain size and mechanical properties (elasticity and damping coefficients). A sufficiently large number of particles is considered to represent the powder size distribution and to account for the coated volume. The coating mechanism is described as a boundary condition setting the particles into motion to fill a space representing the volume above a processing table. In the following sections we summarize the theoretical background of the algorithms used and then present the results obtained for a coating process similar to that used in many commercial powder bed systems.

## Models

Discrete Element Method (DEM) modelling was developed by Cundall and Strack for granular assemblies such as rock formations [20]. It has been adapted for granular flow. The concept of DEM is that every particle of rock, grain of sand, or molecule is treated as an individual, with its own properties, which interacts with other particles which are in range to be affected by it. Cundall and Strack developed their model due to the impossibility of being able to monitor the internal forces of granular assemblies and the problems of calculating such behavior from a finite element method. DEM is a Lagrangian approach where the modelled region considers the particles inside their own point of reference. DEM models use Newton's laws of motion for conservation of momentum (Eq. 3) and angular momentum (Eq. 4).

$$\boldsymbol{m_i}\frac{\boldsymbol{dv_i}}{\boldsymbol{dt}} = \sum_j \boldsymbol{f_{ij}} + \boldsymbol{f_i^b} + \boldsymbol{m_i g} \tag{3}$$

$$I_i\frac{\boldsymbol{dw_i}}{\boldsymbol{dt}} = \sum_j \boldsymbol{m_{ij}} + \boldsymbol{m_i^b} \tag{4}$$

The model used in this paper is a 'soft sphere' model. This means that each particle has a sphere of influence and via overlapping with other particles (or obstacles) a force is generated, proportional to the overlap, which is then resolved to move the particle. Figure 3 (a) shows the force model used in this work dealing with the interactions between particle i and j. Figure 3 (b) defines translational velocities (v) and angular velocities (ω), particle radii (r), normal direction vectors (n) and particle overlap (δ). Four degrees of freedom are present in the model, shown in Figure 3c that allows incorporation of different types of friction (shear, rolling and twist). Full details of the numerical formulation can be found in [21,22].

## Experiments

A Renishaw AM250 machine is utilized to study the coating process and how the powder layer thickness affects build quality. The machine consists of a rigid coater moving at a constant speed to displace

powder from the source to the processing table. LPW Ti-6Al-4V with the powder size distribution shown in Figure 4 is used for all parameter studies.

The experiment consists in running the laser along a line directly onto various depths of Ti-6Al-4V powder using a laser power of 200W, an exposure time of 125µs and a point distance of 75µm (hatch spacing does not apply as the laser was run in a single line, but a typical value used for Ti-6Al-4V is of 150µm). As can be seen from the results in Figure 5, as the powder depth is increased, the melt track becomes unstable and this is thought to be due to Rayleigh-Plateau instabilities.

Measurements would indicate a laser track width of about 82µm which is only marginally higher than the laser diameter, however, it should be pointed out that this was done directly onto the powder, with less heat transmitted vertically it would be expected that the bead would have a higher dome than if melted onto the base plate, where it would run off closing the gaps between tracks slightly more. In normal builds using the same laser settings, relative densities have been measured in the 97-99% range with low porosity identified by micrographs. This would suggest that any holes in the underlying layer are filled by subsequent melt liquid and smoothed by re-melting.

## Rain Model vs. Coating Simulation

Models studying the interaction of the heat source with the powder feed stock rely on the availability of a realistic powder bed geometry that is discretized to obtain further insight in material behavior during phase change and consolidation of the final build material [4,5,6,7,8,23,24,25]. Many of the melt pool models reported in literature rely on numerical creation of powder beds using the rain model or derivatives thereof [26]. The general advantage of the rain model is that it accounts for the feedstock powder size distribution providing powder bed geometries in a very quick manner. Mindt et al. used powder bed geometries obtained from a coating simulation taking the powder size distribution and the coater arm velocity into account. It was shown that the interaction of the coating arm with particles can lead to powder layer inhomogeneity that affects the overall melt pool behavior and the shape of the solidifying material [7].

A domain is defined where powder beds are randomly deposited using the rain model. The same domain is also used to perform a complete coating simulation resolving the coating process. The domain is subdivided into sections where particle distribution statistics can be gathered and compared. Figure 6 compares the predictions of the rain model with two coating scenarios by considering the smallest particles concentration along the powder bed. The powder bed length is subdivided into 10 segments for which the concentrations are calculated. Large differences depending on how the powder bed is created can be observed.

The rain model shows a uniform distribution of the smallest particle diameters along the domain length. The concentration corresponds closely to the prescribed powder size distribution provided as input to the model. The coating models however predicts a segregation of particle sizes during the coating process. As the random powder bed is pushed from the source to the processing table, small particles seem to separate early from the overall powder flow – very much like the behavior observed during flow of granular material [27].

Two coating scenarios are compared in Figure 6. In the first, a layer is deposited using the rain model, then the coater arm is activated to spread a second layer onto the powder bed. In the second scenario three layers are spread one after the other to obtain a similar powder layer thickness as in the first

scenario. Comparing the small particle concentrations it can be deduced that the coating process and its repetitions increases particle segregation leading to a significant reduction of small particles concentration in sections further away from the source. The concentration seems to reach a steady value in the central parts of the studied powder bed before increasing again towards the end of the domain. The concentration in segments 6, 7, 8 and to some extent 9 are very similar. We therefore assume that the predicted packing densities are representative for the central part of the processing table. The increase in the concentration in segment 10 is attributed to domain edge effects.

## Coating Results – First Layer

Experimental observations indicate that the first powder layer spreads differently to later layers. Nevertheless, if we assume that the roughness of a processed region is negligible, we can relate the coating results of the first layer to the behavior on a processed surface. Coating simulations are performed to provide the starting point towards calculating a representative powder layer for further analysis. Figure 7 shows particle distributions of the first layer for both 30 and 50 µm displacements. The most significant difference is the sparsity of particles in the case of 30 µm displacement leading to a very low powder bed packing density. There is also a continuous line where no particles are left on the processing table (corn rowing). Further the particle segregation discussed above dominates the powder distribution. Figure 8 explains these characteristics via a magnification of the gap between the coating arm and the processing table surface. The gap height corresponds to a table displacement of 30 µm. Particles larger than the gap are pushed ahead of the coater blade and cannot be placed on the processing table. They accumulate in front of the coating arm; eventually blocking the gap and reducing the number of particles that remain behind the coater arm.

The same general behavior can be also observed for the 50 µm gap. However since the volume percentage of particles larger than 50 µm is low, the impact is not as large as with the 30 µm gap. It must be noted, however, that the numerical model does not account for crushing of powder particles, pressing particles into the base material or the coater arm notching. These are effects that are likely to take place in the real machine when the gap size is too small compared to the powder particle sizes. Also the numerical coater arm will exert as much force as needed to fulfil the motion boundary condition. This occasionally leads to the squeezing of some of the large particles, that they can pass the gap as if they were rubber balls.

In order to extract statistical information about the numerical powder beds a 10x5 raster is imposed on the numerically distributed powder layer. Within each unit box the number of particles of each of the size classes and the packing density is calculated. Figure 9 compares 3D carpet plots of the powder packing density for the studied displacements. The 30 µm plot shows lower packing densities with large fluctuations corresponding to the gap blocking observed above. The 50 µm plot shows a general decline of the packing density toward the far end of the processing table. This is due to the segregation of small particles that leads to higher packing densities in the first sections of the powder bed. The change in packing density in coating direction is no longer visible after approx. 40% of the studied domain length. It can be assumed that the average packing density in the rest of the powder bed is representative for the real process.

To obtain a good representation of the packing density only the central sections are averaged. The 30 µm displacement leads to an average packing density of 20%; whereas a displacement of 50 µm leads to

a packing density of around 38%. These values are lower than 50-55% as predicted by rain models[23,25].

The displacement (gap size) is varied in Figure 10 to identify conditions under which higher packing densities can be obtained for the first layer or on solidified surfaces. The packing density seems to reach an asymptotic value of approx. 50% for displacements larger than 200 µm. This is attributed to the mechanical interaction of the particles among themselves leading to segregation of particle sizes and reduced flowability.

The coater velocity is varied from a minimum value of 4 to 12.5 mm/s. The average packing density for the lowest and maximum coating velocities were found to be 35 and 35.6% respectively. For the conditions and the powder size distribution studied the coating velocity does not seem to have a significant influence on the powder packing density.

## Coating Results – $n^{th}$ Layer

When spreading a new layer of powder on previous layers, new particles encounter different conditions depending on the status of the underlying material. If the new layer is being spread onto unprocessed powder particles numerical simulations show that the new layer induces a motion of previously existing particles in the same direction as that of the coating arm. The motion of all particles (previous layer and newly coated) leads to further segregation of particle sizes (as shown in Figure 6) as well as the opening of spaces allowing for larger particles to pass easier under the coater arm. The problems related to larger particles blocking the gap between the coater arm and the processing bed surface are not as dominant when coating a new layer on unprocessed powder as during first layer or on a solidified surface.

Figure 11 shows the packing density distribution for 4 coating cycles. The packing density is calculated on a 10x5 raster across the powder bed. The four layers were created using one 50 µm layer followed by three 25 µm processing table displacements. In between coating steps the powder layers were not melted, so the example is representative for a region where the heat source is not activated. The packing density reaches a max. of 30%. A linear trend line is included providing a means for quick assessment of the packing density to be expected. Extrapolating the results beyond the number of layers studied here will probably lead to unrealistic results. The variation of estimated packing density is large for the first layer and decreases as more layers are coated. Within the number of layers studied the summation of multiple small displacements we do not achieve the packing density of large displacements as can be deduced by comparing Figure 10 and Figure 11.

In the previous discussion we assumed that if the surface roughness of a processed surface is negligible, then coating the first layer is comparable with the coating of a processed surface. However, if the surface roughness is large, then particles moving over a processed (solidified) area will experience an increased resistance to their motion. Particularly high protrusions may retain particles leading to areas not being coated. Figure 12 shows the particles of a freshly spread powder layer on top of a processed surface. The solidified surface was numerically calculated using the same melt pool models described in[6,7,8]. The solidified volume was reused as the substrate for the coating of a new powder layer. The new particle diameters are scaled down to see through the new powder layer. The solidified surface finish – displayed as a triangulated surface - shows material beading leading to high rises as well depressions that affect the coating behavior. The new powder particles seem to stop around these

restrictions leading to a reduced availability of new particles around the surface rise. Smaller particles seem to trickle into depressions. Such inhomogeneity is expected to happen throughout the powder bed in a complex interaction between the powder spreading mechanism and surface roughness. The result is large variations in the packing density from one area to the other.

## Process Modelling

The numerical powder beds are transferred to melt pool models aiming at the characterization of the melt pools and process window [6,7,8]. The models include the geometry of the powder bed and the substrate as well as a part of the chamber to capture gas flow above the processed surface. Navier Stokes equations are used to model Laser powder interaction, heat transfer via conduction and convection as well as fluid flow in the melt pool. The momentum equations are extended with gravitational body forces and surface tension including Marangoni forces. The energy equation is extended with radiation source terms and accounts for phase change. Different samples of powder beds are considered to investigate the influence of the powder bed structure on the processed surface.

Figure 13 shows a sample of a 50 µm powder bed with the corresponding deposition strategy used in the experiments discussed above. The sample was chosen to include regions where multiple particle clusters can be found as well as regions where the coating was not very successful leaving the substrate free of any new particles. In regions where a large cluster of small particles can be found (e.g. lower right corner of sample) the melt pool surface is fairly uniform showing small variations in height. The processed material is however connected to partially molten particles that will contribute to the side wall roughness of the final product. The triangular region on the left of the specimen powder bed did melt and solidify without being filled by neighboring melt pools. The resulting depression is in the order of 20 µm, which will lead to increased powder layer thickness in the next coating step. Finally it is interesting to note the melt pool structure around the large particle on the right hand side of the specimen powder bed. This particle does not fully melt. Surface tension forces lead to a complex surface structure around this particle; with a fairly steep decline in build height near the particle.

The process was repeated for three layers, where the deposition track is rotated by 67$^{o}$ every layer. Figure 14 shows the resulting build shape. Each layer is colored by a different color. The left image shows the top view of the last layer numerically processed. The right image shows a side view of the built layers and how they interconnect giving a solid body. The tracks are rotated around the geometry center line. The numerically predicted structure closely resembles that of Figure 5a. The main lines are visible as continuous bead lines that are connected where the melt pools are large enough to touch. The connection between the beads is however not continuous leading to the wavy structure shown in Figure 5 (experiments) and Figure 14 (numerical result). The results show standalone and partially molten particles in regions where the connection between beads is not complete. The numerical build suggests that such regions also exit inside the product as can be seen in the side view where the laser track misses a region leaving a “hole” in the build.

## Conclusions

A discrete element model is developed to investigate the coating process of powder bed processes. Modelling the coating process suggests average powder bed packing densities around 40%. In certain situations where the space below a rigid coating arm is smaller than the larger particles being spread the packing density can be significantly lower. Inhomogeneity of coated powder bed leads to increased surface roughness of the deposited material. Results indicate that increased surface roughness leads to

continued spread inhomogeneity that may lead to areas having very thick powder layers. The combined results of the coating and melt pool models provides insights in process parameter interaction and predict similar surface structures as those observed in micrographs.

## Acknowledgement

The authors acknowledge the financial support of the European Commission 7th Framework Program AMAZE. The authors would like to also thank project partners and collaborators for the ongoing discussions, support and motivation.

## Captions

Figure 1: Evolution of powder layer thickness for different table displacements assuming a uniform packing density of 50%

Figure 2: Powder layer thickness as a function of packing density

Figure 3: (a) Force model. (b) Distance and velocity definitions. (c) Degrees of freedom in the model.

Figure 4: LPW Ti-6Al-4V powder size distribution

Figure 5: Results from single line experiment (E3)

Figure 6: Comparison between rain model, one coating layer and multiple coating layers showing how the smallest particle diameter concentration is affected by the coating process

Figure 7: First layer particle distribution on processing table for two displacements

Figure 8: Magnification of gap between coating arm and the processing table for a vertical table displacement of 30 □m

Figure 9: Packing density distribution for a 10x5 raster across the numerical powder bed for 30 (left diagram) and 50 □m (right diagram) table displacements.

Figure 10: Packing density as predicted by coating model for different gap sizes

Figure 11: Packing density distribution for a 10x5 raster across the numerical powder bed after 4 layers: 1x100 + 3x25 µm table displacements.

Figure 12: Powder layer spread on previously processed surface

Figure 13: Powder bed and processing strategy (left) and final surface shape after processing (right)

Figure 14: Resulting build shape after 3 layers, each rotated by 67°: Left image shows the top view of the numerical build. Right image shows a side view of the numerical build

## References


1. I. Yadroitsev: *Selective Laser Melting*, LAP Lambert Academic Publishing, Saarbrücken, 2009.
2. C.D. Boley, S.A. Khairallah and M.A. Rubenchik: *Appl. Optics*, 2015, vol. 54, no. 9, pp. 2477-2482.
3. A. Rubenchik, S. Wu, S. Mitchell, I. Golosker, M. LeBlanc and M. Peterson: *Appl. Optics*, 2015, vol. 54, no. 24, pp. 7230-7233.
4. C. Körner, E. Attar and P. Heinl: *J. Mat. Proc.*, 2011, vol. 211, pp. 978-987.
5. C. Körner, A. Bauereiß, E. Attar, *Modeling Simul. Mater. Scie. Eng.*, vol. 21, no. 085011, 18pp.
6. N. N'Dri, H.-W. Mindt, B. Shula, M. Megahed, A.D. Peralta, J. Neumann and P. Kantzos: *TMS 2015 Supplemental proceedings*, p. 338, Wiley, New Jersey, 2015.
7. H.-W. Mindt, M. Megahed, A.D. Peralta and J. Neumann: (2015) DMLM Models: *22nd International Symposium on Air Breathing Engines - ISABE*, Oct. 25-30, Phoenix, AZ., USA.
8. H.-W. Mindt, M. Megahed, B. Shula, A. Peralta and J. Neumann: *AIAA Science and Technology Forum and Exposition*, San Diego. In: AIAA 2016-1657.
9. J. Ding, P. Colegrove, J. Mehnen, S. Ganguly, P.M. Sequeira Alemeida and F. Wang: *Comp. Mat. Sci.*, 2011, vol. 50, no. 12, pp. 3315-3322.
10. R. Martikanitz, P. Michaleris, T. Palmer, T. DeRoy, Z.K.Liu and R. Otis: *Additive Manufacturing*, 2014, vol. 1, no. 4, pp. 52-63.
11. L. Papadakis, A. Loizou, J. Risse and J. Schrage: *Procedia CIRP.,* 2014, vol. 18, pp. 90-95.
12. L. Papadakis, A. Loizou, J. Risse, S. Bremen and J. Schrage: *Virtual and Physical Prototyping*,

2014, vol. 9, no. 1, pp. 17-25.

13. N. Keller and V. Ploshikhin: *1st International Symposium on Material Science and Technology of Additive Manufacturing*, 2014, Bremen, Germay.
14. N. Keller and V. Ploshikhin: *Solid Freeform Fabrication Symposium*, 2014, Austin, Texas.
15. J.C. Heigl, P. Michaleris and E.W. Reutzel: *Additive Manufacturing*, 2015, vol. 5, no. 9, pp. 9-19.
16. E.R. Denlinger, J.C. Heigl and P. Michaleris: *Journal of Engineering Manufacture,* 2014, vol. 1, pp. 1-11.
17. P. Michaleris: *Finite Elements in Analysis and Design*, 2014, vol. 86, pp. 51-60.
18. J.A. Slotwinski, E.J. Garboczi, P.E. Stutzman, C.F. Ferraris, S.S. Watson and M.A. Peltz: *J. Res. of National Institue of Standards and Technology*, 2014, vol. 119, pp. 460-493.
19. J.A. Slotwinski and E.J. Garboczi: *Jour. of Mat*., vol. 67, no. 3, pp. 538-543.
20. P.A. Cundall and O.D.L. Strack: *Geotechnique*, 1979, vol. 29, no. 1, pp. 47-65.
21. M.A.J. Holmes: *A numerical simulation of particulate distribution of the blast furnace raw materials burden through the Paul Worth bell-less top apparatus,* 2015, Ph.D. Thesis, University of Swansea.
22. M. Holmes , R. Brown, P. Wauters, N. Lavery and S. Brown: *App. Math. Mod*: 2015, vol. 40, no. 5-6, pp. 3655-3670.
23. E. Attar: *Simulation der selektiven Elektronenstrahlschmelzprozesse*, 2011, Ph.D. Thesis, Erlangen
24. I. Kovaleva, O. Kovalev and I. Smurov: *Physics Procedia*, 2014, vol. 56, pp. 400-410.
25. W.E. King, A.T. Anderson, R.M. Ferencz, N.E. Hodge, C. Kamath and S.A. Khairallah: *Applied Physics Reviews*, 2015, vol. 2, no. 041304.
26. P. Meaking and R. Jullien: *J. Physique*, 1987, vol. 48, pp. 1651-1662.
27. G. Metcalfe and M. Shattuck: *Physica A*, 1996, vol. 233, pp. 709-717.
28. C. Li, C.H. Fu, Y.B. Guo and F.Z. Fang: *Procedia Manufacturing*, 2015, pp. 1-11.

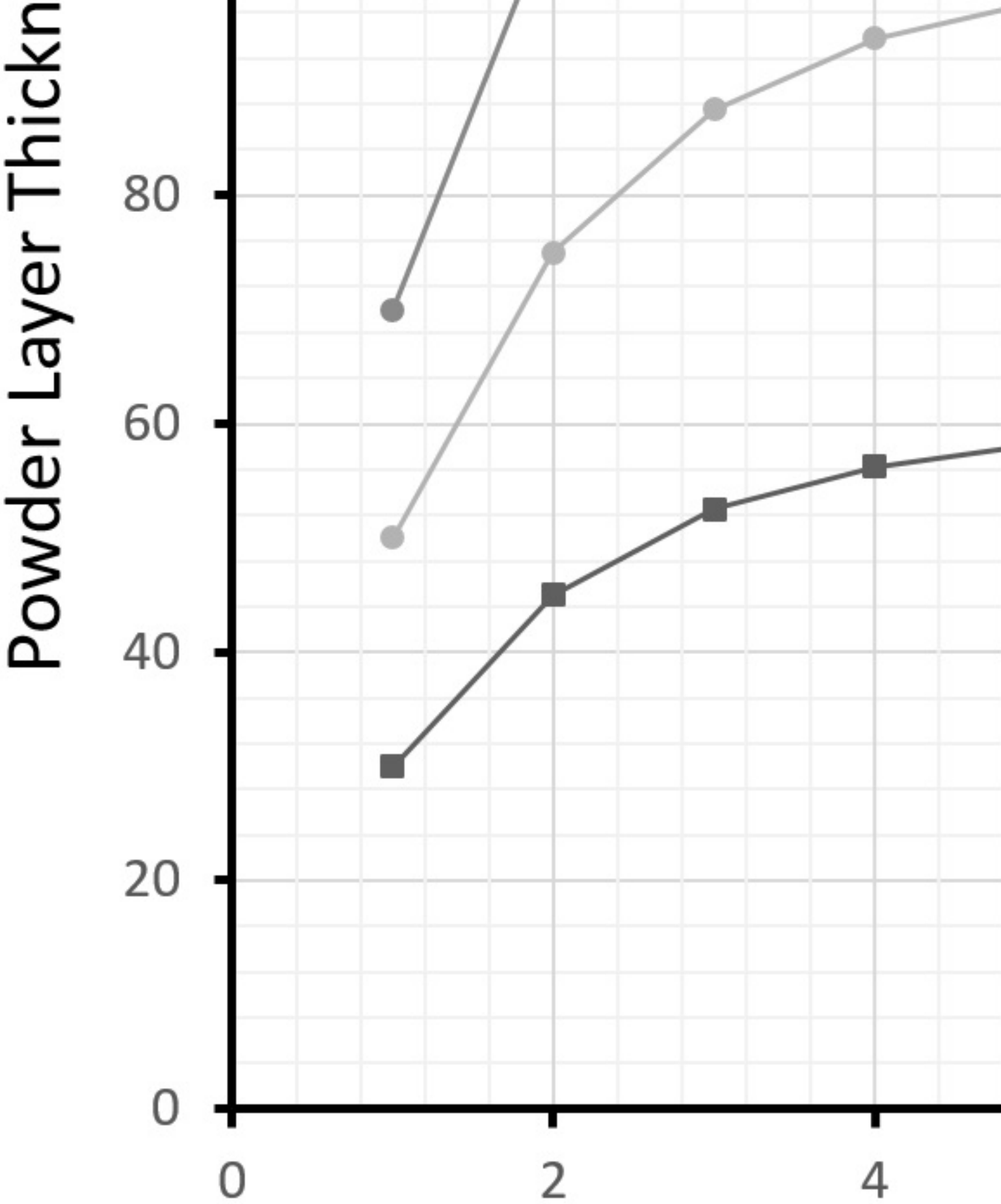
Powder Layer Thickn
80
60
40
20
0
0
2
4

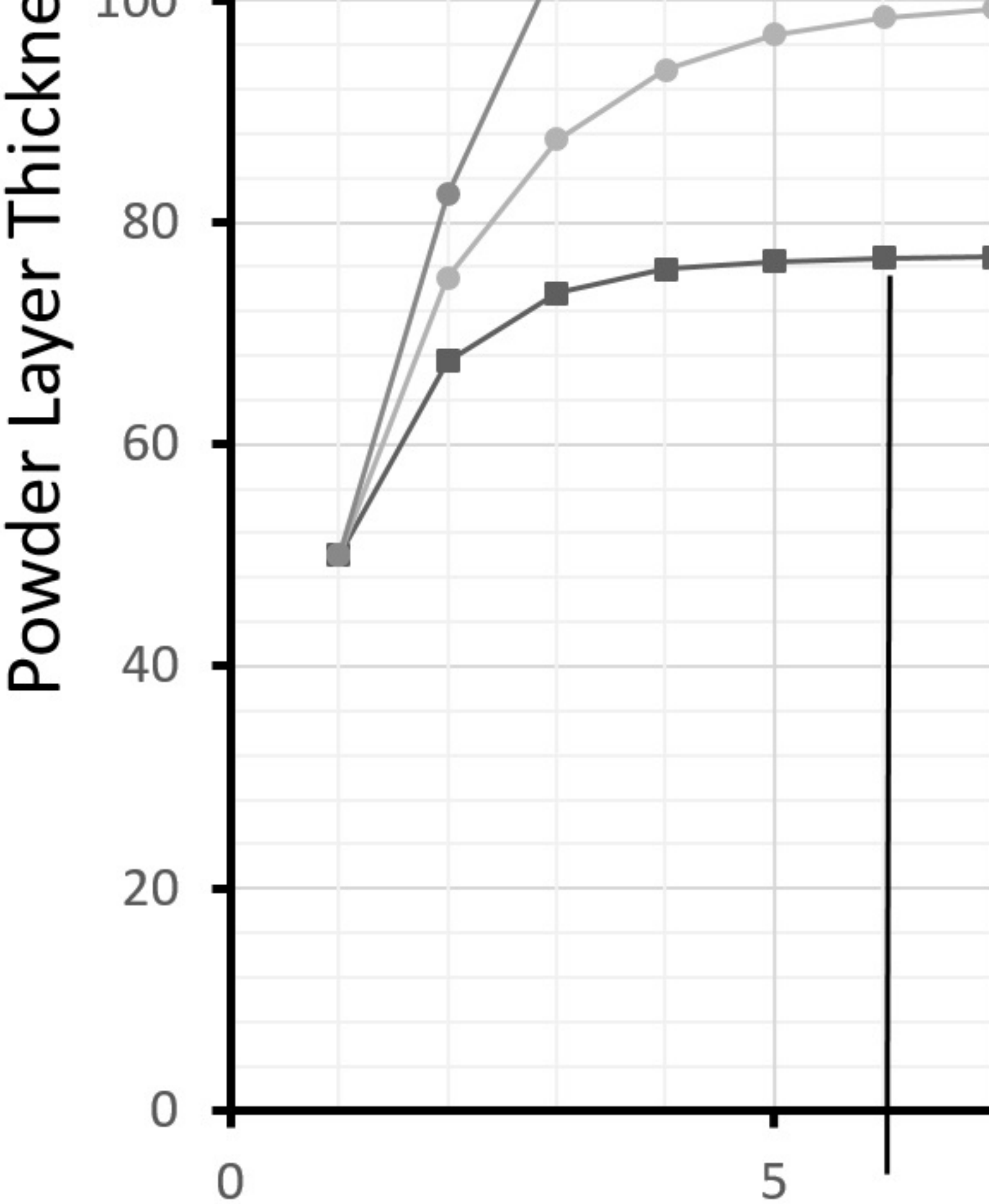
Powder Layer Thickne
100
80
60
40
20
0
0
5

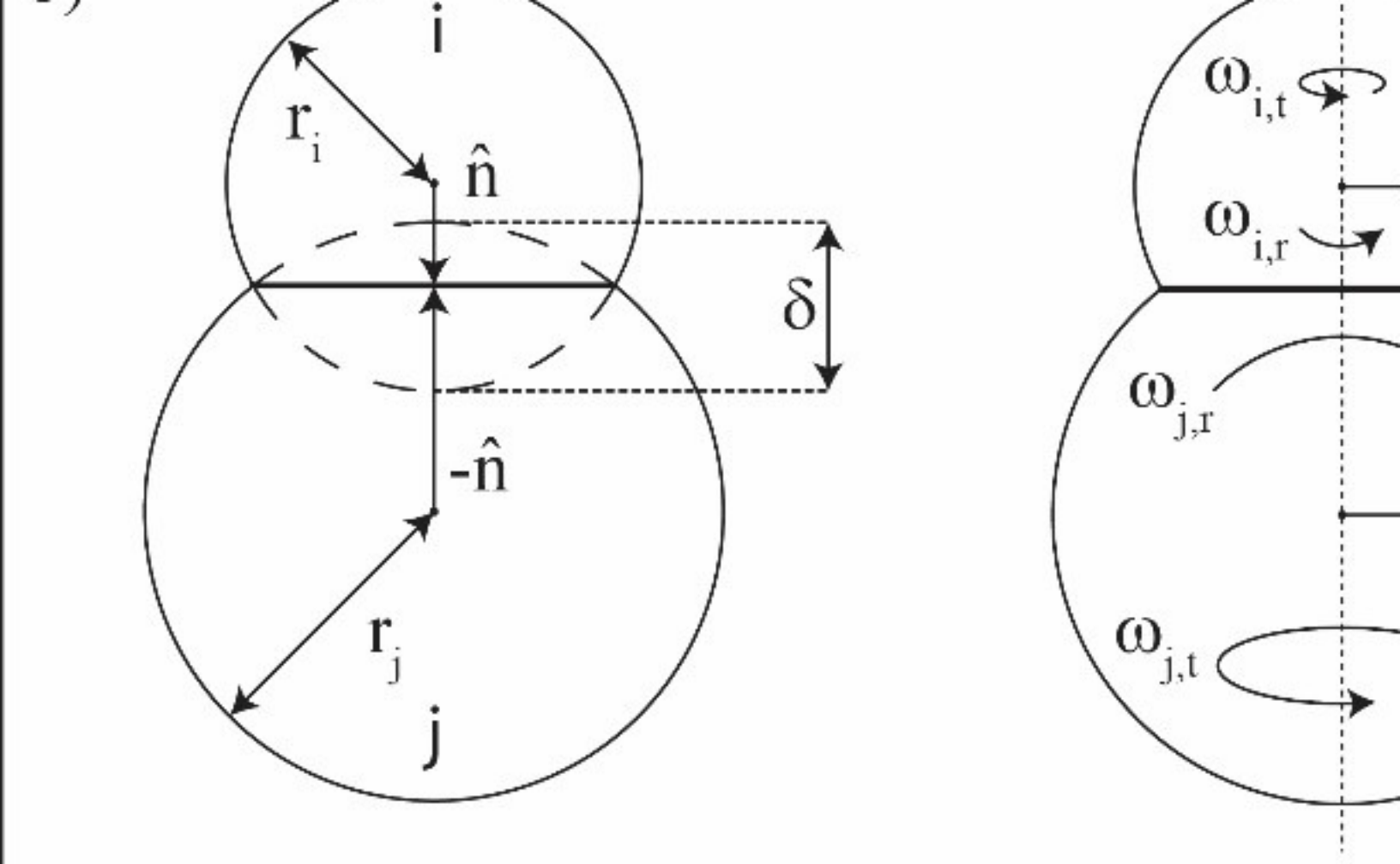


c)

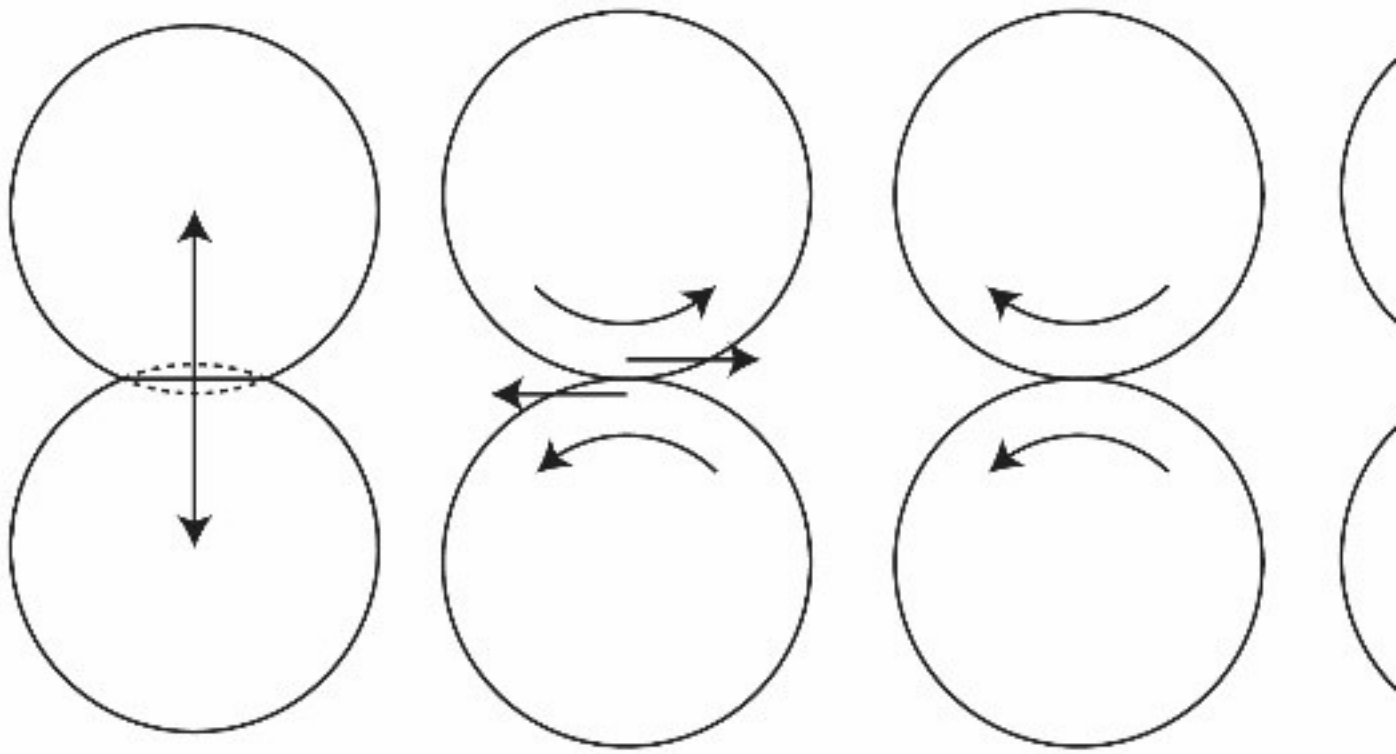

Normal Shear Rolling

| Comp. | Ti | Al | V |
|---|---|---|---|
| %wt. | 91 | 5.5 | 3.5 |

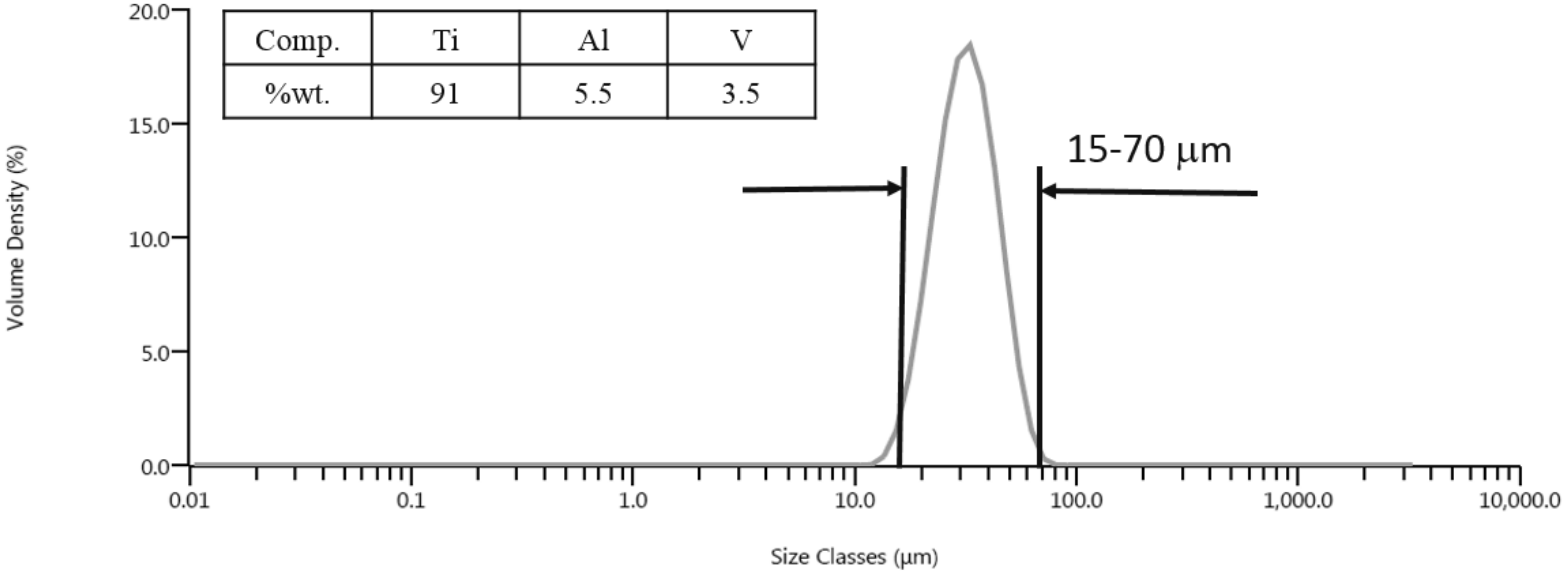

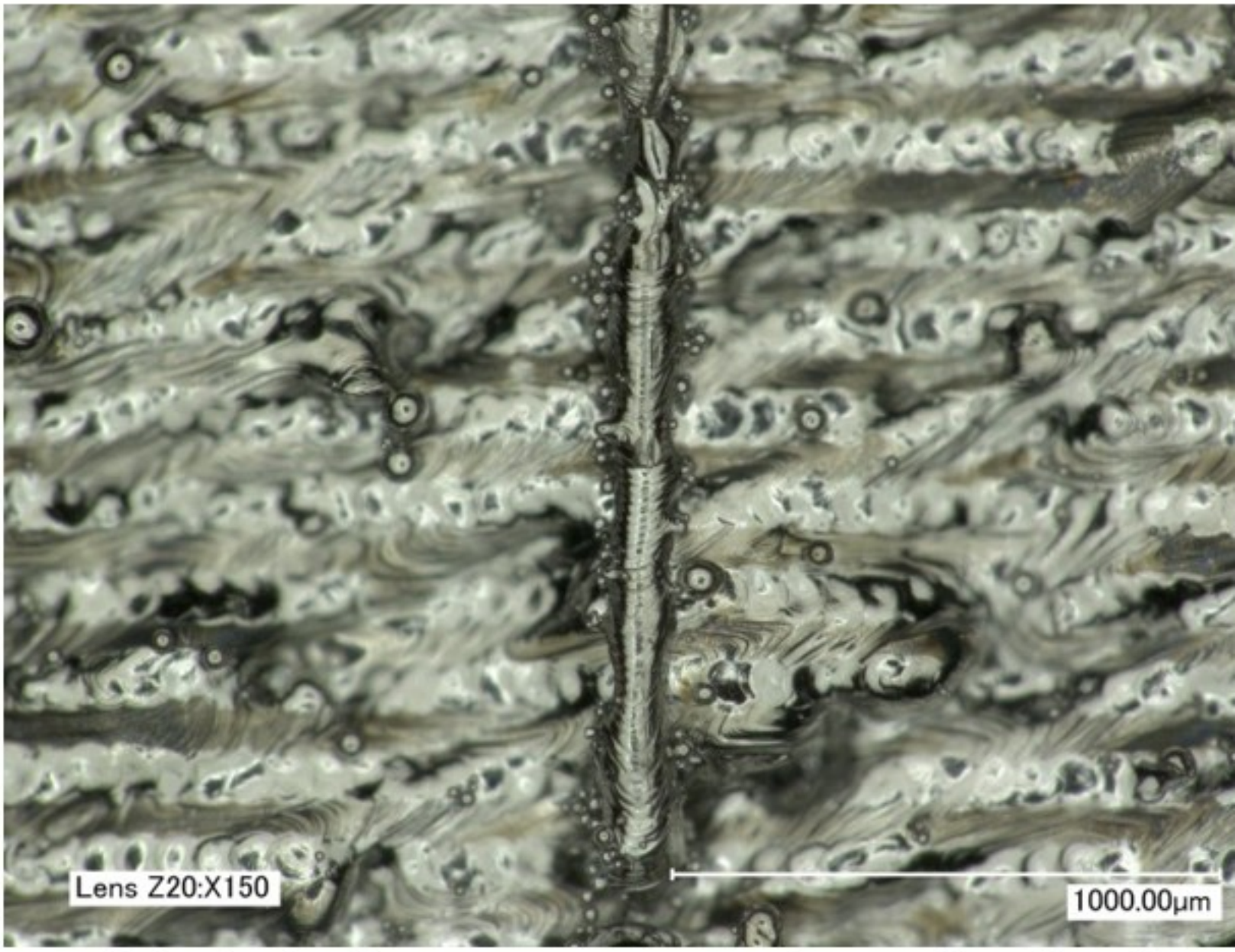


(a) Single line onto 50 µm of powder depth

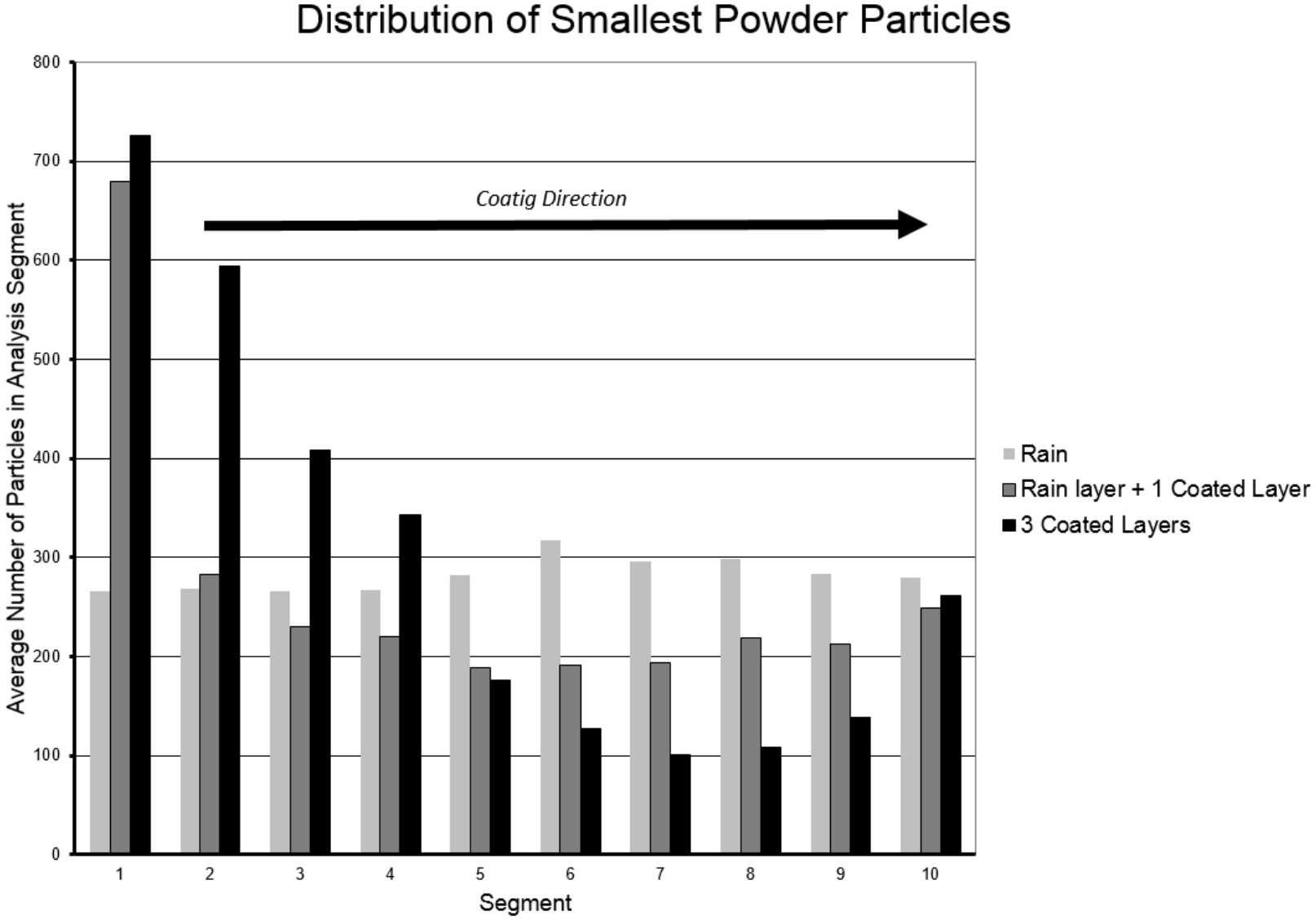
Distribution of Smallest Powder Particles
Average Number of Particles in Analysis Segment
800
700
600
500
400
300
200
100
0
Coatig Direction
1
2
3
4
5
6
7
8
9
10
Segment
Rain
Rain layer + 1 Coated Layer
3 Coated Layers

*Table displacement [$\mu m$]*

*First lay*

30



Source

50

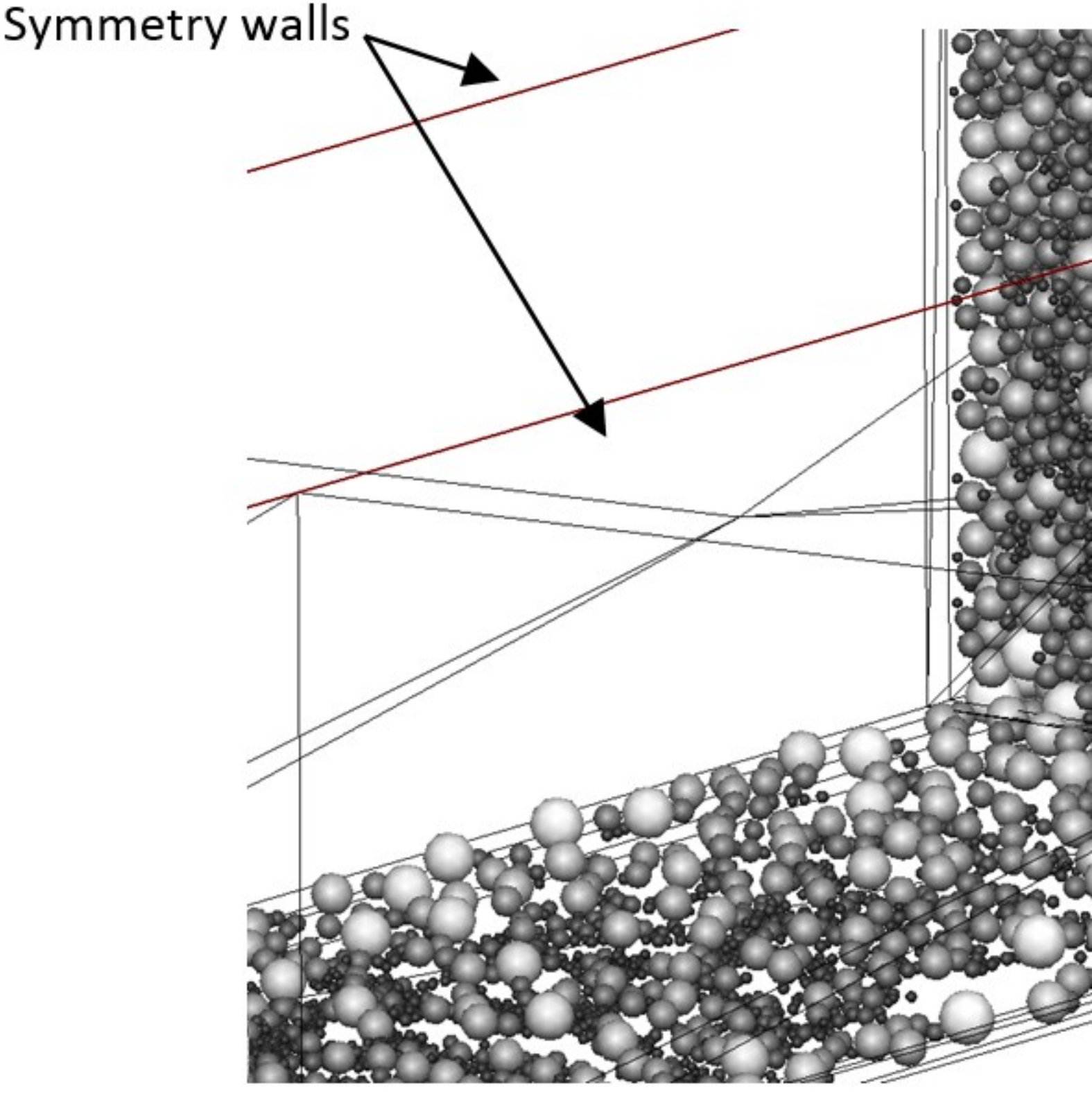
Symmetry walls

*Table displacement [μm]*

*First layer powder packi*

30

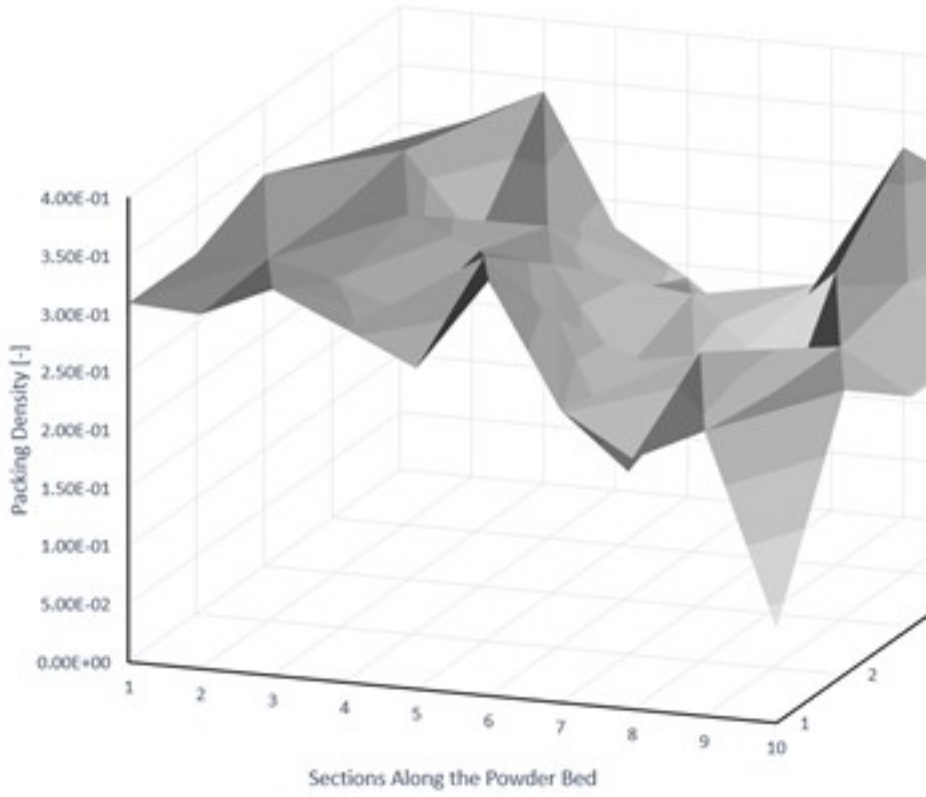


*Coating directio*

50

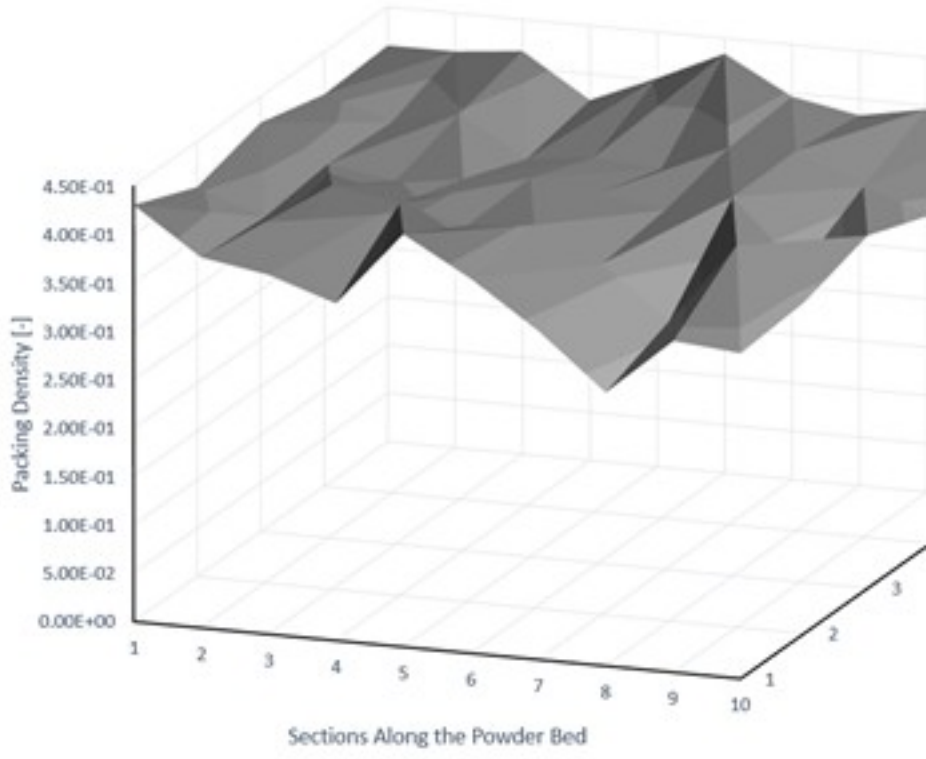

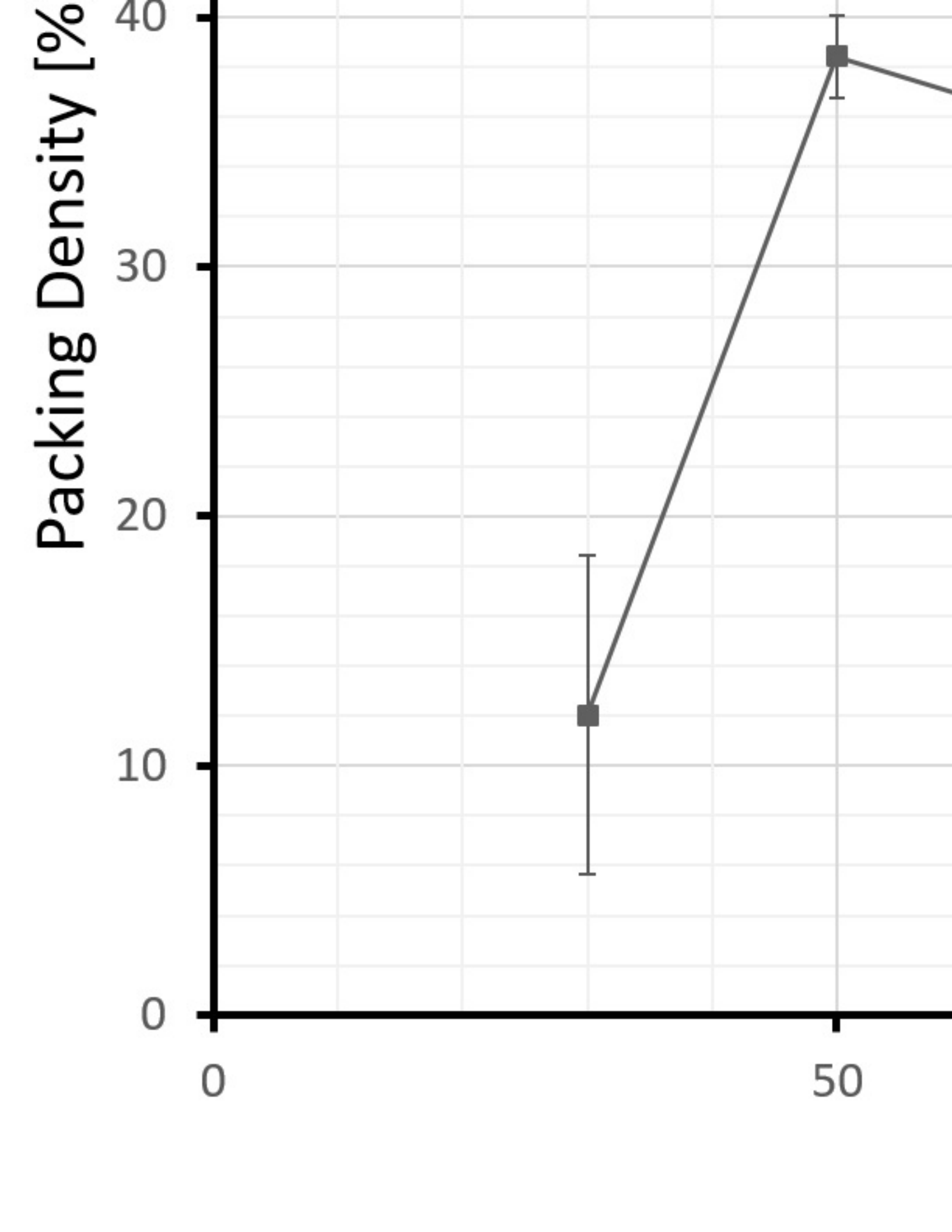
Packing Density [%
40
30
20
10
0
0
50

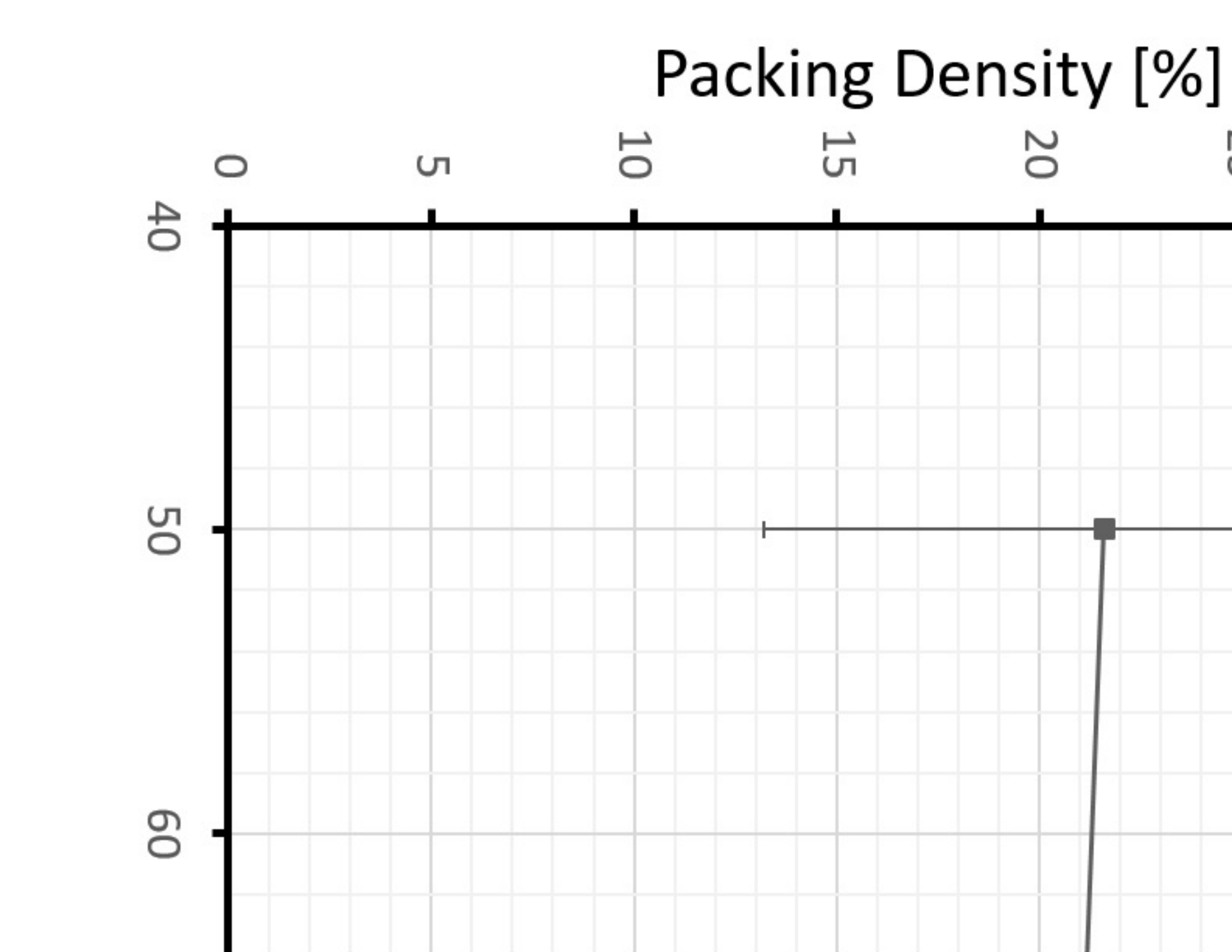
Packing Density [%]
0
5
10
15
20
40
50
60

Surface rise with no coating and subsequent reduced particles deposition

Small particle
accumulated in v
between several

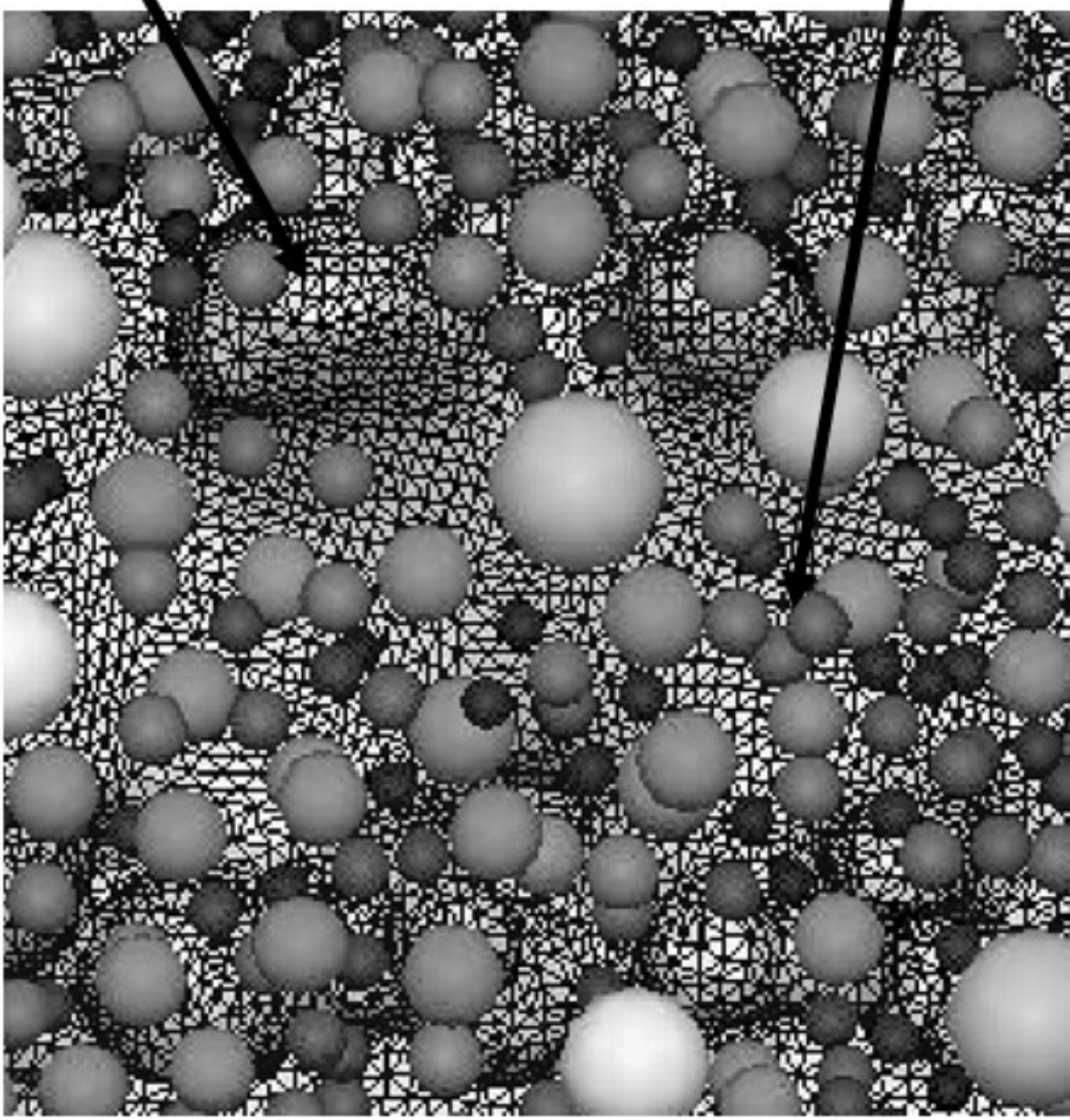

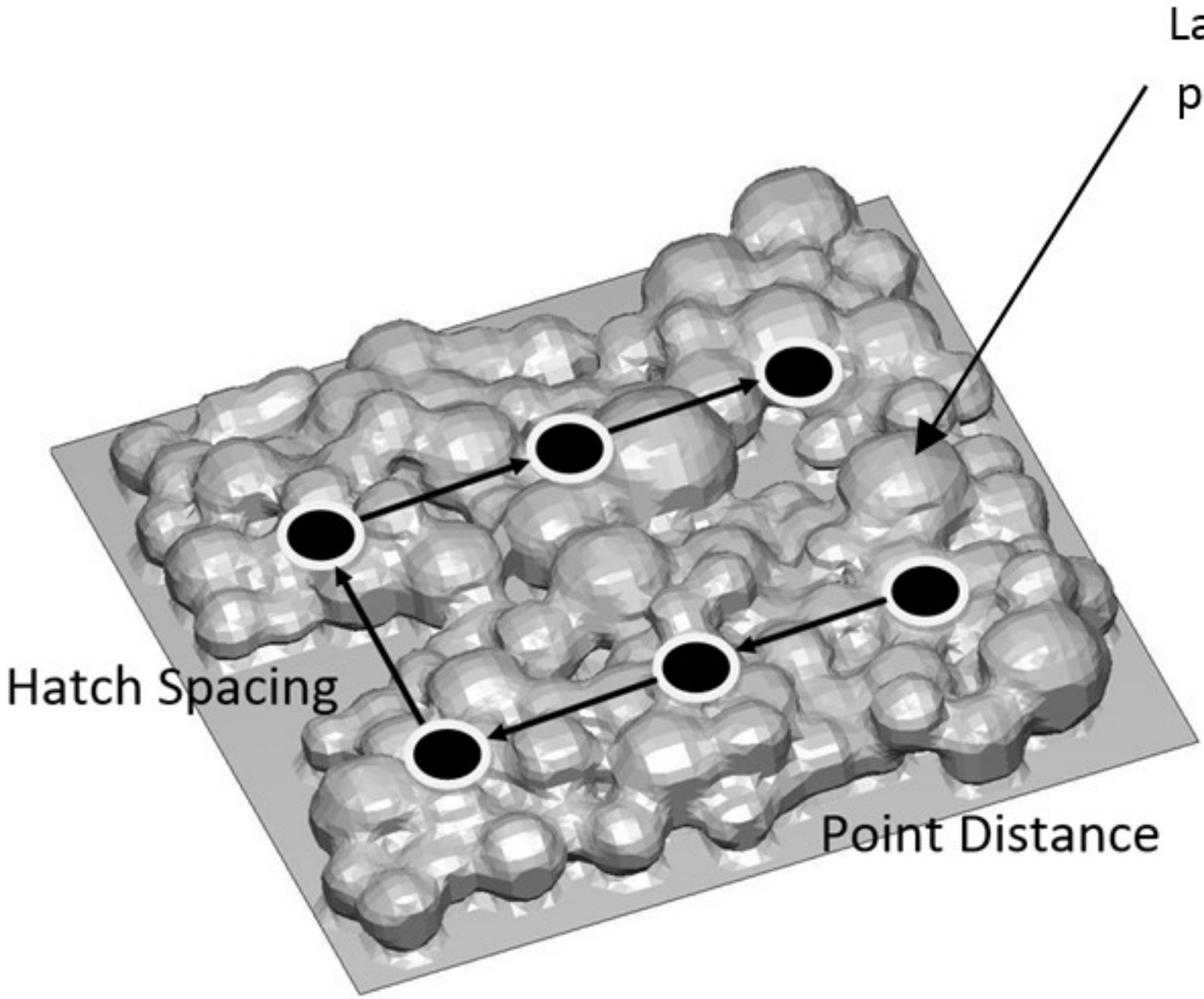
La
p
Hatch Spacing
Point Distance